DESIGN SPACE EXPLORATION OF CENTIMETER-SCALE WIND TURBINES USING A PHYSICS-MODIFIED OPTIMIZATION FORMULATION

D. Rancourt *

Aerospace Systems Design Laboratory
Guggenheim School of Aerospace Engineering
Georgia Institute of Technology
Atlanta, Georgia 30332, USA

C. Landry

Université de Sherbrooke
Sherbrooke, Québec, J1K 2R1, Canada

L. Fréchette

Microengineering Laboratory for MEMS
Department of Mechanical Engineering
Université de Sherbrooke
Sherbrooke, Québec, J1K 2R1, Canada

D. N. Mavris

Aerospace Systems Design Laboratory
Guggenheim School of Aerospace Engineering
Georgia Institute of Technology
Atlanta, Georgia 30332, USA

ABSTRACT

This paper explores the design space of centimeter-scale micro wind turbines to power wireless sensors through an experimentally validated modeling and simulation environment. A stochastic optimizer is used to obtain a functional relationship between the minimum wind velocity required to find a feasible design and multiple constraints relevant to turbine designers, such as the maximum turbine radius, electrical power required, minimum voltage required and available generators. This relationship is created from an optimization formulation that uses knowledge from the underlying physics and previous optimizations. It is shown that the design space of micro wind turbines is significantly different than large wind turbines due to the low Reynolds number regime. Also, a strong coupling exists between the choice of generator and optimal wind turbine geometry to minimize the wind required to meet the requirements. Smaller generators are more appropriate for micro wind turbines only if a constraint is applied on the maximum radius of the turbine and if no minimum voltage is required for a fixed power output.

Keywords: Micro wind turbine, Self-powered sensors, Autonomous sensors, Energy harvesting, Wind energy.

1. INTRODUCTION

Society's interest for miniature wireless sensors to monitor environmental parameters has grown significantly in the last decade [1,2]. Maximizing the knowledge about parameters such as temperature, pressure, wind speed, toxicity of air, location of people or general building functions are the founding principles of smart buildings [3], smart cities, and smart grids. The objective is to install these sensors in large numbers, anywhere from the top of a building down to an air duct to measure air properties or even to detect when a filter needs to be replaced. As these sensors are mainly installed in areas where it is hard to reach, they must have a lifespan of several years without requiring maintenance. They must be self-powered to avoid the burden of replacing the battery and avoid any negative environment impacts, especially if they are widely used. Installation cost can also be reduced significantly by transmitting data using wireless signals. This setup enables the use of thousands of these low cost sensors within a small area. Figure 1 shows a generic block diagram of self-powered autonomous sensors as described by Sardini [4].

The power level generated from the external source is generally too low to power the sensor and wireless transponder continuously. A DC-DC converter boosts the voltage and the power management stores this energy for transient operation. This component also

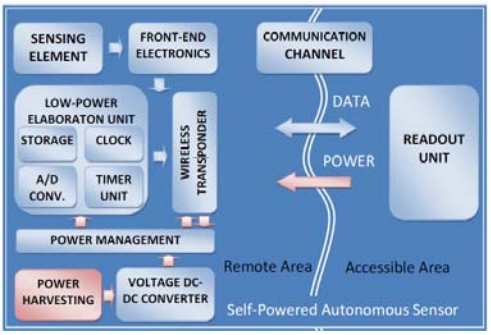


Fig. 1 Block diagram of self-powered autonomous sensors [4]

* Corresponding author (david.rancourt@gatech.edu)

DOI : 10.1017/jmech.2014.23
Copyright © 2014 The Society of Theoretical and Applied Mechanics, R.O.C.
https://doi.org/10.1017/jmech.2014.23 Published online by Cambridge University Press

distributes the power to the wireless transponder and other electronic components. This architecture allows the wireless sensor to transmit data at a variable frequency, depending on the power available. Most uses of these sensors do not require continuous monitoring. An average supply of a few milliwatts is usually enough to power the transponder every minute for duration of about a second [4], although recent improvement in technology allows micro transceiver to transmit continuously with only 3mW [5].

Different energy sources can be used to power wireless sensor nodes such as wind, sunlight, mechanical, thermal [6] and nuclear [7], but the choice of the energy source is a function of its availability [8], reliability and cost. Recently, nuclear batteries were proposed to power sensor nodes due to their reliability and low maintenance, but their cost is still prohibitive for widespread usage. For indoor and outdoor usages, wind from air ducts or from the environment is one of the most promising sources of energy due to its high power potential. The average wind velocity in the 50 largest cities in United States is 4m/s (standard deviation of 0.6m/s) [9] while air duct wind velocity can range anywhere between 3m/s and more than 15m/s [10]. If off-the-shelf components such as small plastic propellers and simple DC generators are used, then the system can be very low cost and meet the power requirements.

The efficiency of micro wind turbines is significantly lower than large wind turbines which can operate very close to the maximum theoretical power using complex devices such as variable pitch and active load control to optimize efficiency at all operating conditions [11]. According to the Betz limit [1], the maximum efficiency that can be achieved is 59.3% for an ideal wind turbine. However, mainly due to the viscous losses and tip losses, the maximum demonstrated efficiency is about $C_p = 48\%$ [12]. The use of gearboxes between the propeller and generator allows to partially decouple the design of these two components to optimize the efficiency at the design point. Miniature wind turbines do not have these advantages; they operate at much higher angular velocity in an unfavorable Reynolds number range with fixed propellers and no gearbox.

Although the design of micro wind turbines poses significant challenges, the first demonstrations of functional micro wind turbines using direct drive electromagnetic generators coupled to a plastic propeller of a few centimeters were done in the early 2000's by Federspiel *et al* [13]. Rancourt *et al* [14] analyzed the effect of blade twist on the performance (on and off-design) of the propeller and the whole system. A 4.2 cm prototype was tested with an overall efficiency of 1.5% at 5.5m/s and 9.5% at 11.8m/s with a conventional DC motor. Figure 2 presents the propeller efficiency and a picture of the propellers analyzed. Although it was demonstrated that low tip-speed [2] ratio propellers are more suitable for micro wind turbines, no optimization was done to demonstrate how to improve the

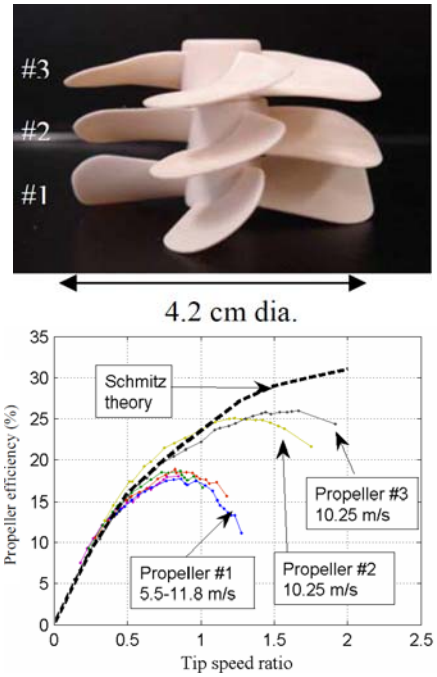


Fig. 2 Propeller efficiency for 3 propeller designs as a function of tip-speed ratio [14]

efficiency of the whole system or what generator characteristics are favorable.

In 2010, Xu *et al* [15] proposed a model to analyze the efficiency of a coupled propeller/generator using an equivalent circuit approach with a simplified friction model for the generator. The model was validated using off-the-shelf components, including a 7.6cm propeller and DC generator. An overall efficiency of 14.8% was predicted and the operating range was between 3 and 4.5m/s. The same year, Carli *et al* [16] performed a theoretical analysis to optimize the coupling between the generator and AC-DC converter to maximize the power conversion over a wide range of operating condition. Vlad *et al* [17] proposed some controls solution to maximize the mechanical to electrical conversion for generators used at partial loads. These optimization efforts demonstrated the necessity to take into account the efficiency of the propeller, the generator and the electronics at full and partial loads to access the efficiency of the overall system. However, no work was done to better understand the design space to help designers select the appropriate components for specific applications.

Sardini [18] and Flammini [19] both demonstrated the feasibility of a fully autonomous system that includes the wireless data transmission powered by a micro wind turbine. Wind velocity and air temperature readings were transmitted over a few meters once every 2 seconds [18]. They both used commercially available components but Flammini [19] compared the efficiency of three different motors around a fixed propeller design. To get this stable power supply, a DC-DC converter is usually used to either step up the voltage or reduce it. Flammini [19] proposed that it is possible to step up a voltage as low as 0.6V. As electronics improve, this number is likely to decrease. Recent de-

[1] The Betz theory predicts the theoretical limit of a wind turbine for an unshrouded rotor using a momentum approach.

[2] The tip-speed ratio is the tangential tip speed over the free stream velocity W

https://doi.org/10.1017/jmech.2014.23 Published online by Cambridge University Press

velopments in electronics allow voltages as low as 20mV to be increased using a resonant circuit [20] with an efficiency that is highly dependent of the input voltage. Any voltage below this threshold cannot be used by the system and is therefore lost.

Although most research used off-the-shelf components and optimized a subset of the whole system, Holmes *et al* proposed a sub-centimeter [21] diameter micro wind turbine with an integrated generator. A few years later, Howey *et al* [22] designed an optimal wind turbine and generator combination for on-design performance able to operate with an airflow as low as 3m/s, producing 80μW and 2.5mW at 7m/s. Advanced manufacturing techniques were used in both cases to create the optimal propeller and generator. Although the designs are very efficient for their size, the manufacturing techniques could not be used for large-scale production.

A critical parameter to be minimized in the design of micro wind turbines is the wind speed required W given a set of constraints such as power required, minimum voltage, maximum blade radius, and generator properties. One the minimum wind velocity is obtained for this specific application and generator selection, the optimal wind turbine can be obtained using a modeling and simulation environment and a simple optimizer.

This paper presents the design space exploration of micro wind turbines coupled with an electromagnetic generator to provide guidelines on the design of propellers and selection of generators. The objective is to evaluate the feasibility of micro wind turbines under constraints such as the maximum diameter, minimum voltage, power required, and generator properties using an optimization formulation that minimizes the number of function calls. First, the optimization formulation based on surrogate models and a stochastic optimizer is detailed. Then, the physics-based modeling and simulation environment and the experimental validations are presented. Finally, the results section is separated into two parts. The aerodynamic performance of micro propellers is analyzed first followed by the study of the sensitivity of the minimum wind required to the generator selection and requirements.

It is shown that the design space of micro wind turbines is significantly different than that of large wind turbines due to high airfoil drag. First, on and off-design performance of the wind turbine only is presented. Second, constraints on the geometry of the turbine such as the maximum diameter allowable are shown to significantly affect the optimal generator for a minimum wind velocity design. Finally, this paper shows that large generators are more suitable for wind turbines optimized for minimal wind velocities and low power only if no constraint is applied on the diameter.

2. METHODOLOGY

The proposed methodology aims at obtaining a functional relationship of the minimum wind required to obtain a feasible propeller design that can meet a set of requirements under constraints. This relationship is complex and expensive to obtain as it is not the output of most available aerodynamic and generator codes. The methodology uses surrogate models [23], design of experiments and a specially-formulated optimizer to minimize the computational cost to obtain the relationship.

Most aerodynamic codes provide a relationship of the torque produced by a wind turbine as a function of the turbine geometry and operating conditions. These results are then inputs to a generator model to obtain the electrical power and voltage produced by a wind turbine in a specific operating condition. The modeling and simulation environment used in this project, detailed in Section 3, can provide the power and voltage produced as a function of a set of design variables such as generator properties, wind turbine geometry, and operating conditions as presented in the following equations. The blade chord and blade twist are both implicit variables: They are optimized to maximize the efficiency at the design condition.

$$P = P(\text{generator properties}, r, \omega, W, b) \tag{1}$$

$$V = V(\text{generator properties}, r, \omega, W, b) \tag{2}$$

However, these relationships do not inform the engineer about the sensitivity of the design to a change in the requirements, or help them to select the optimal generator for their applications, because these parameters are mixed between the design variables and the responses. An inverse of Eqs. (1) ~ (2) would directly provide the engineers the effect of a change in the requirements of the optimal turbine. However, such a functional relationship does not exist as there are multiple solutions for a fixed set of requirements. An alternative is to obtain an equation of the minimum wind velocity W required to find a feasible design as a function of the salient requirements and constraints met by engineers, as presented in Eq. (3). Once it is found that a feasible design exist by comparing the the minimum wind velocity required W and the wind available for a specific application, it is relatively easy to obtain one or multiple designs that can meet the requirements.

$$W = W(\text{generator properties}, P_{req}, V_{\min}, r_{\max}) \tag{3}$$

One must note that this equation is not an equivalent to efficiency conversion of the wind turbine, as the disk area is an implicit variable. A structured design of experiments (DoE) where each experiment (denoted i) is the result of a single objective optimization problem, as detailed in Eq (4). A design of experiment consists of purposeful changes to the inputs (design variables) to a process in order to observe the corresponding changes in the outputs in an intelligent way.

$$\begin{aligned} &\text{Given (generator properties)}_i,\ P_{req,i},\ V_{\min,i},\ r_{\max,i} \\ &\text{Minimize} \quad W_i \\ &\text{with respect to} \quad r,\ \omega,\ W,\ b \\ &\text{subject to} \quad P\text{-}P_{req,i} = 0 \\ &\qquad\qquad r_{\max,i}\text{-}r \le 0 \\ &\qquad\qquad V_{\min,i}\text{-}V \le 0 \\ &\qquad\qquad \text{Bounds of the model variables} \end{aligned} \tag{4}$$

https://doi.org/10.1017/jmech.2014.23 Published online by Cambridge University Press

There are three continuous variables and one discrete variable (number of blades). The quasi-inversion of Eqs. (1) ~ (2) is expensive and requires a very high number of function calls due to the multiple optimizations. Therefore, a surrogate model of Eqs. (1) ~ (2) should be used by the optimizer instead of calling the aerodynamic and generator codes directly, which are significantly more expensive to run.

The optimization formulation stated thus far does not reuse the results from previous optimizations (each experiment of the DoE is independent). It is known that an optimized turbine which is designed for a higher power output leads to a non-decreasing wind velocity if all the other design variables are kept fixed:

$$W(P_{req1}) \geq W(P_{req2}) \tag{5}$$

$$\text{if } (P_{req1} > P_{req2})$$

If a full factorial design of experiments [23] on P_{req} is run in an order such that all the parameters are kept fixed and the power required is increased between two experiments ($P_{req,i} > P_{req,i-1}$), an extra inequality constraint is added which reduces the design space to find a feasible design.

$$U_{b,W} \geq W_i \geq W_{i-1} \tag{6}$$

In Eq. (6), i represents the index of the case in the design of experiment, $U_{b,W}$ is the upper bound on the wind velocity and W_{i-1} is the wind velocity found in the previous experiment. For the degenerative case for which no feasible design is found for experiment i (a higher wind velocity would be required than the upper bound), all the following experiments with fixed parameters (except the increasing power requirements) are simply removed.

Figure 3 presents a conceptual view of the design of experiments for 10 levels in the power required P_{req} and associated responses ($W_{\downarrow}i$) with all the other parameters fixed. The dashed line represents the minimum velocity needed to obtain a feasible design for a fixed power required. For the lowest value of power required, the whole range of wind required is included in the optimization. However, for $P_{req,i+1}$, the lower bound on wind velocity in the optimization becomes W_i, the minimum wind velocity from the previous optimization. This process is repeated until the maximum value of P_{req} or that the design space collapses. It the latter case, the experiments with a higher power required are discarded as they are unfeasible.

In summary, the power and voltage equations are converted to a single objective function, the minimum wind velocity required to find a feasible design as a function of a set of requirements, such as minimum voltage and power required. This proposed methodology recycles the results from previous experiments to shrink the bounds on the wind velocity during the optimization and in some cases, infer that a specific experiment is unfeasible without performing the experiment.

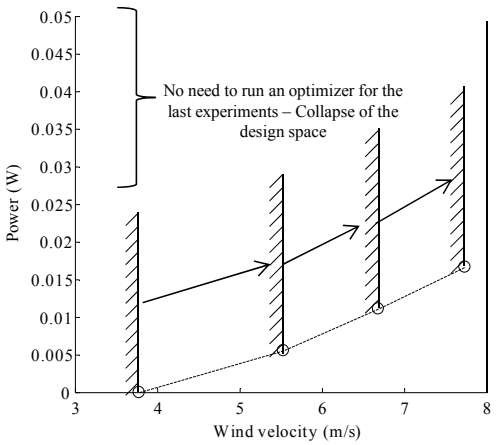


Fig. 3 Effect of using the results of the prior experiment on the lower wind velocity bound for the next experiments

3. MODELING AND SIMULATION ENVIRONMENT

3.1 Micro Wind Turbine Performance Prediction Model

The modeling and simulation environment used to analyze the mechanical power produced by micro wind turbines uses two open-source codes, QMILL and QPROP [3]. The first code provides an optimal propeller geometry given the design conditions and general propeller characteristics (design tool). The second code analyzes the propeller with different angular velocity and wind velocity given you provide the details of the blade geometry (analysis tool). Both codes are based on an extension of the classical blade-element/vortex formulation with radially varying self-induction velocity and circulation. This method is well adapted for heavily-loaded actuator disks [24] such as wind turbines. The change in airfoil drag coefficient in the code is considered through Eq. (7):

$$Cd(C_l, Re) = \left(Cd_0 + Cd_2(Cl - Cl_{cd0})^2\right)\left(\frac{Re}{Re_{ref}}\right)^{\mathrm{Re}_{\exp}} \tag{7}$$

where the coefficients can be calibrated experimentally or using aerodynamic codes on airfoil sections. Figure 4 details the general modeling and simulation architecture built around these codes to predict the shaft torque produced by the wind turbine. This generic architecture allows on-design and off-design analyses of micro wind turbines.

3.2 Generator Model

The generator model assumes a simple DC motor model [24,25] which demonstrated its applicability in previous work [14]. This model relates the angular velocity, torque and generator properties to the electrical power and voltage. The internal resistance is

[3] http://web.mit.edu/drela/Public/web/qprop/

https://doi.org/10.1017/jmech.2014.23 Published online by Cambridge University Press

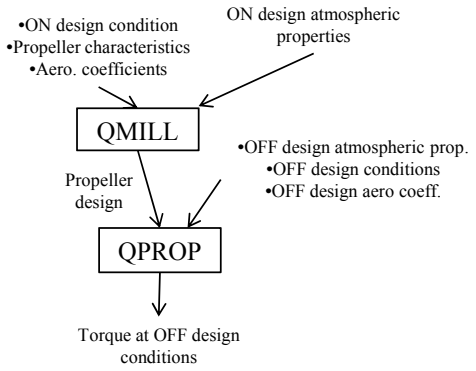


Fig. 4 Modeling and simulation environment architecture for torque prediction

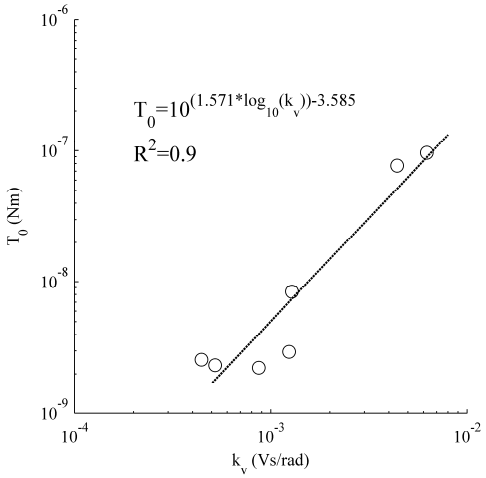


Fig. 5 Constant friction term as a function of the electromagnetic constant for the analyzed motors

assumed to be constant as the coil temperature does not increase for these low power settings. Two sources of friction are considered: Constant friction and viscous friction as shown in Eq. (8).

$$T_f(w) = T_0 + \omega K_F \tag{8}$$

A wind turbine produces axial loads on its bearings as a function of wind velocity, disk area, and design tip-speed ratio. In a simple experiment where the axial load is varied for multiple angular velocities, it was demonstrated that the thrust affects the friction by up to 25% for a propeller with the largest disk area, operating in the upper range of the wind velocity considered in this study. However, high thrust loads are also correlated to a high power generated by the propeller, minimizing the relative importance of the increase in friction to only a few percent on the electrical power. Therefore, this parameter can be neglected in this preliminary analysis. The current produced by the generator can be derived from Eq. (9) and the voltage at the motor terminals from Eq. (10).

$$i(T_m, \omega) = \frac{T_m - T_f(\omega)}{k_t} \tag{9}$$

$$V(i, \omega) = k_v \omega - Ri \tag{10}$$

4. MODEL CALIBRATIONS

4.1 Motor Characterization

The internal resistance R of the motor is the average of the measured resistance at 6 different angular positions. The voltage constant k_v is obtained by spinning the generator by another motor and dividing the open circuit voltage by the angular velocity. For brushed DC motors, k_t and k_v are approximately equal [25]. The relation between the friction and angular velocity is obtained from a no-load run, where all the torque is dissipated into friction. The speed was measured from the frequency of the electrical pulses using an oscilloscope (Agilent Technologies DSO6014A 100Mhz). Appendix A presents the list of motors considered in this study with their respective parameters and Fig. 5 illustrates the relation between k_v and the constant friction term T_0. All these motors are low cost, off-the-shelf components mainly used in mobile phones or model airplanes. It is observed that k_v is dependent on the internal friction of the motor mainly due to the increase in size of the motors.

4.2 Aerodynamic Coefficients

The modeling and simulation environment is calibrated by minimizing the errors between the power predictions and the experimental validation for one propeller. Then, the performance of another propeller is predicted and compared to experimental results to validate the calibration.

4.2.1 Experimental Set-up

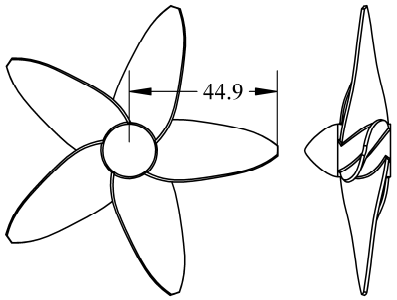
The propellers are manufactured from plastic (ABS) using a 3D printer (Dimension Elite) with a resolution of 0.005 in. No improvement on the propeller finish is done or rebalancing. Propellers are held on the generator by a simple interference fit assembly. The wind tunnel is open-loop with a test section of 0.6m by 0.6m. The wind velocity is measured using an anemometer (ALNOR GGA-26) with a precision of 0.1m/s. The wind turbine assembly is held in the middle of the test section by a single 3/8 in diameter shaft.

To control the angular velocity of the propeller and measure its torque for a fixed wind velocity, the Speed 265 generator was used as sensor. The control on the angular velocity is done by varying the load on the generator and the angular velocity is measured using an oscilloscope. The torque generated by the propeller is derived using Eq. (9) given that the generator internal friction $T_f(\omega)$ is known from no-load spin tests. Table 1 details the salient characteristics of the propellers where propeller #2 was used for the calibration and #1 for the validation. The airfoil is a 5% cambered plate with a constant thickness of 1mm. A drawing of the two propeller geometries is presented in Fig. 6.

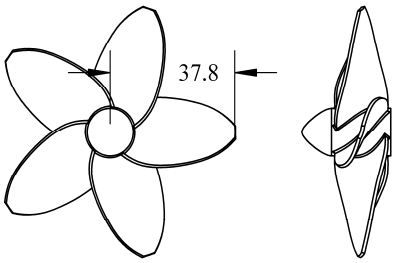
https://doi.org/10.1017/jmech.2014.23 Published online by Cambridge University Press

Table 1 Main characteristics of the 2 propellers developed for the calibration and validation of the model

ID	R (cm)	b	λ_d
1	4.49	5	2.59
2	3.78	5	1.99



(a) Propeller # 1



(b) Propeller # 2

Fig. 6 Propeller geometries for the calibration and validation (dimensions in mm)

4.2.2 Calibration

The aerodynamic parameters are calibrated using two sources of data: Low speed wind tunnel tests on airfoils and the wind tunnel tests of propeller #2. All the parameters in Table 2 except Cd_0 are obtained by analyzing the work of Sunada [26], Pelletier [27] and Shyy [28] on low speed airfoils in the Reynolds number range of 4,000 ~ 60,000. At the design condition, the airfoil at 50% of the radius of propeller #1 operates at a Reynolds number of 7,000 at 2,200rpm. Propeller #2 operates at approximately a Reynold number of 6,000 at the design condition. Both propellers were also operated at over 5,000rpm. The design lift coefficient is assumed to be 0.5, which is approximately the maximum lift-to-drag ratio of the airfoil.

The reference drag coefficient Cd_0 is calibrated by minimizing the sum of the square of the errors of the electrical power generated by propeller #2 while the other coefficients are kept constant. The error is minimized with a Cd_0 of 0.07. The lift at zero angle of attack Cl_0 did not need calibration. Figure 7 presents the power predicted versus the wind tunnel tests for propeller #1 after calibration. The validation of the code using the wind tunnel tests of wind turbine #1 is presented in Fig. 8.

Table 2 List of calibrated aerodynamic coefficients

Aerodynamic parameters	Values
Cd_2	0.09
Cl_{cd0}	0.3
Re_{ref}	20,000
Re_{exp}	–0.3
Cl	5.4
Cl_{des}	0.5
Cd_0	0.07
Cl_0	0.25

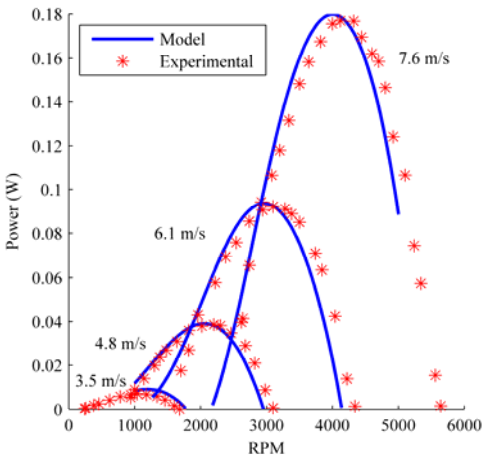


Fig. 7 Calibration of the model using propeller #2

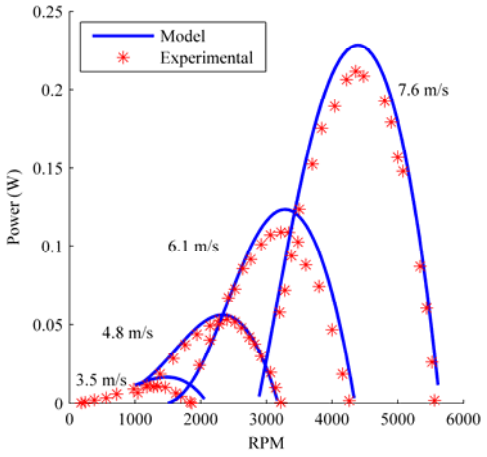


Fig. 8 Validation of the model using propeller #1

For propeller #2 at 4,000rpm, normal atmospheric conditions and an axial velocity of 7m/s, the Reynolds number is approximately 13,500 at 50% of the radius, which translates to an actual airfoil parasitic drag of 0.078. From Eq. (8), the same airfoil at a Reynolds number of 4,000 would have a parasitic drag coefficient of 0.11, which is about 50% higher than what was published by Sunada [26]. It must be noted that the losses associated with viscous drag on the wind turbine hub is included in the parasitic drag of the blade. For Reynolds number around 50,000, the predicted drag coefficient falls a few percent beside the experimental values obtained by Pelletier [27].

https://doi.org/10.1017/jmech.2014.23 Published online by Cambridge University Press

This calibration assumes a fixed thickness-to-chord ratio. However, Sunada [26] demonstrated that a change in the thickness ratio from 2.5% to 5% increases the parasitic drag coefficient by up to 35% for a cambered plate. If the thickness to chord ratio has to be increased due to manufacturing constraints for high tip-speed ratio designs and small diameter, the reference parasitic drag coefficient should be adapted accordingly.

5. MECHANICAL AND ELECTRICAL POWER

5.1 Implementation of the Surrogate Model

A surrogate model of the mechanical power is required for two reasons. First, it significantly reduces the computational expense of the optimizer presented in Eq. (4) and it allows the designers to easily visualize the trends and sensitivity to a change in the constraints. A surrogate model of the mechanical power is preferred to a surrogate model on the electrical power and voltage to reduce the dimensionality of the problem, as the mechanical-to-electrical power conversion relationship is known. Table 3 presents the bounds of the design variables. The reference parasitic drag coefficient Cd_0 (see Eq. (5)) is added to calibrate the model but assumed fixed for the later optimization.

A total of 50,000 uniformly distributed experiments were initially created without considering the design tip-speed ratio and operating tip-speed ratio constraints. Then, a filter was applied to enforce the tip-speed ratio constraints, which reduced the number of experiments down to 12,000. Although this number is still relatively high, the computational time to run the experiments was under 6 hours. An artificial neural network (ANN) surrogate model form is selected for its capability to represent highly non-linear problems. SAS Institute JMP^{TM} statistical software was use to fit a two layer surrogate model with 11 hyperbolic tangent nodes per layer. The training and validation data sets had a R^2 of 0.994 and 0.990 respectively with a mean absolute error on the mechanical power prediction under 5mW (2% of the range).

5.2 Results

5.2.1 On-Design Propeller Efficiency

The turbine is designed and operated at a given design tip-speed ratio λ_d. A wind velocity of 5m/s and a turbine radius of 3.5cm are assumed fixed and the tip-speed ratio is modified by varying the angular velocity. Although this method includes the effect of Reynolds number, the effect was found to minimal for the purpose of capturing general trends.

Figure 9 shows the propeller efficiency as a function of the design tip-speed ratio and Cd_0, where the optimal design tip-speed ratio as a function of Cd_0 is represented by a dashed line. It must be mentioned that each coordinate on the graph is a different propeller design, always operated at the design condition. The conversion efficiency from wind power to shaft power of micro wind turbines is generally low due to the highly viscous flow at these Reynolds number and due to the manufacturing constraints. As for large wind turbines [11], the efficiency of micro wind turbines increases with diminishing airfoil parasitic drag. The maximum propeller efficiency is around 26.5% for a Cd_0 of 0.07 (from the calibration process). The conversion efficiency is maximized at low design tip-speed ratio for high drag airfoils, while an increase of a few percent in efficiency can be obtained at higher tip-speed ratio for low drag airfoil. For $Cd_0 = 0.07$, the optimal design tip-speed ratio is about 1.7 with a maximum efficiency of 26%. This estimation is also in line with previously published results from Rancourt and al [14] as shown in Fig. 2.

Table 3 Bounds on the design and operating parameters for the mechanical power surrogate model

Characteristics	Lower bound	Upper bound
Design wind velocity W_d (m/s)	3	8
Operating wind velocity W (m/s)	3	8
Design angular velocity ω_d (rpm)	1,000	10,000
Operating angular velocity ω (rpm)	1,000	10,000
Propeller radius R (cm)	2	5
Number of blades b	3	6
Reference parasitic drag coef. Cd_0	0.04	0.1
Design tip-speed ratio λ_d	0.8	3.8
Operating tip-speed ratio λ	$0.4\lambda_d$	$2\lambda_d$

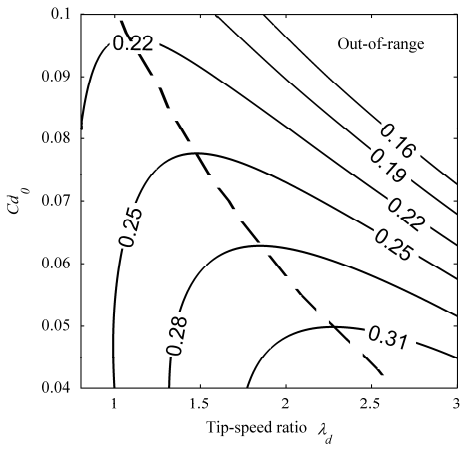


Fig. 9 On-design propeller efficiency as a function of the design tip-speed radio and Cd_0

Although a high design tip-speed ratio is more appropriate for low drag airfoils, the torque is greatly reduced. Figure 10 shows the normalized torque as a function of the design tip-speed ratio and Cd_0. The effect of the airfoil drag on the torque from a fixed diameter turbine optimized for maximum efficiency is almost invariant for low tip-speed ratio.

https://doi.org/10.1017/jmech.2014.23 Published online by Cambridge University Press

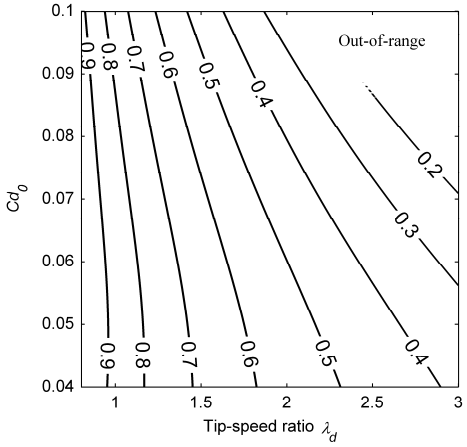


Fig. 10 Normalized torque as a function of λ_d and Cd_0

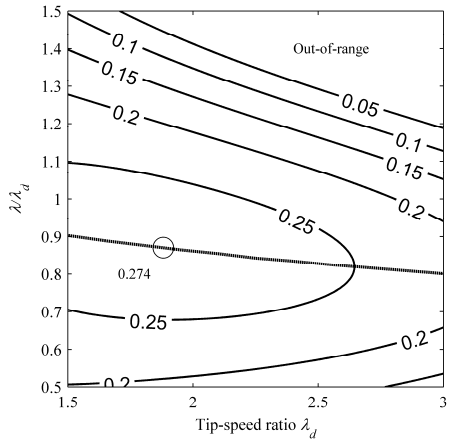


Fig. 11 Off-design propeller efficiency ($Cd_0 = 0.07$)

5.2.2 Off-Design Propeller efficiency

Figure 11 presents the effect of off-design operations on the efficiency of a micro wind turbine with $Cd_0 = 0.07$. The geometry of the propellers remains fixed along the vertical axis, but changes along the horizontal axis. A value over 1 on the vertical axis means that the propeller is operated at a higher tip-speed ratio than the design value.

The optimization of the propeller for a fixed tip-speed ratio is done with a fixed target airfoil lift coefficient of 0.5 as this value maximizes the airfoil lift-to-drag ratio. However, the power losses due to parasitic drag is reduced slightly if that same blade (optimized for $(C_l / C_d)_{max}$ at a given angular velocity) is operated closer to

$$\frac{C_l^{3/2}}{C_d} \tag{11}$$

by reducing its angular velocity , and increasing the lift coefficient at each airfoil section. Therefore the efficiency of the wind turbine increases slightly if $\lambda/\lambda_d \leq 1$ where λ_d assumes that the airfoils operate at the maximum lift-to-drag ratio. Turbines optimized for high tip-speed ratio are more sensitive to off-design operation compared to designs optimized for low tip- speed ratio. The maximum efficiency, including off- design operation is 27.4% at $\lambda/\lambda_d = 0.88$ compared to 26.5% for on-design operation.

6. MINIMUM WIND VELOCITY REQUIRED TO OBTAIN A FEASIBLE DESIGN

This section presents the implementation of the methodology that allows the designers to quickly analyze the feasibility of using a micro wind turbine as a function of a set of constraints and power requirements.

6.1 Implementation of the Surrogate Model

The minimum wind velocity surrogate model is obtained by using an optimizer for each experiment, as shown in Section 4. The role of this model is to allow the visualization of the results and observe the trends. If the wind available is known by the designer, then it is not required to go through the process of creating this second surrogate; the optimization process in Eq. (4) can be done only once. A full factorial design of experiment with parameters presented in Table 4 is used, where α_f is the average static and dynamic friction coefficient ratio compared to the Speed265 generator. The range on the V_{min} is driven by the requirements of power electronics to be supplied by a minimum voltage. The range on the generator property variables were selected based on the available generators and the radius limit based on the manufacturing constraints, as well as the limits of the model.

A large portion of the design space is infeasible, meaning that it is impossible to produce a certain power level with the constraints detailed in Table 3. Therefore, it is required to capture accurately the wind required curve as a function of power required while keeping the other parameters fixed. The number of cases to be run was reduced by more than 25%, by using the data recycling methodology for the optimizer presented in Section 4. Due to previous analyzes it was possible for the algorithm to infer that that it is not required to run the case (of the design of experiment), therefore reducing the computational expense. For more than 75% of the other cases, the wind velocity lower bound for the optimizer was reduced by using prior knowledge (see Eq (6)).

For each of these experiments, a genetic algorithm with population size of 200 was used with a maximum of 100 iterations. The tolerance on the electrical power required is 1mW while a tolerance of 0V was applied for the voltage required. The total computational time on a Intel i7-2600 quad-core computer was 6.3 hours. It must be noted that optimality is not guaranteed with a heuristic optimizer, but due to the multimodality of the response, this type of optimizer is appropriate. The high population number and maximum number of iterations reduce the chances of significantly missing the optimum for each experiment.

A neural network surrogate model form is selected with 11 hyperbolic tangent nodes per layer. The training and validation data sets have a R^2 over 0.99 with a mean absolute error on the minimum wind of 0.09m/s.

https://doi.org/10.1017/jmech.2014.23 Published online by Cambridge University Press

Table 4 Bounds on the design variables for the surrogate model of the minimum wind required

Design variables	Lower bound	Upper bound	Number of levels
V_{min} (V)	0	1.5	4
k_v (Vs/rad)	0.0008	0.008	4
α_f	0	1.2	4
R_{max} (cm)	2	5	4
P_{req} (W)	0	0.05	20

6.2 Results — Coupled Propeller/Generator

This section presents the effect of the electrical power required, minimum voltage, generator selection and radius constraints on the minimum wind velocity required to get a feasible design. The analysis assumes on-design performance with the calibration parameters described in subsection 4.2.2. First, the effect of the minimum voltage and power required on the minimum wind velocity for two different generators is presented in Fig. 12.

For both generators, an increase in the power required leads to an increase in the minimum wind required to find a feasible design within the bounds of the model. This observation is in agreement with Eq. (6). For the RM1a generator, the increase in minimum power from 10mW to 50mW with a minimum voltage of 0.5V increases the wind required from 3.3 to 5.2m/s. On the other hand, the RPM2 generator is a lot more sensitive to changes in electrical power requirements. For generators with a small voltage constant and high internal resistance such as the RPM2, a high angular velocity is required to meet the requirements. However, as the design tip-speed ratio is bounded by the strong drop in efficiency, the turbine radius is reduced, which also reduce the power available from the wind. Generators with higher electrical constant such as the RM1a generator do not need a high angular velocity and are therefore less affected by the increase in power required. The effect of the minimum voltage required is also clearly seen with the RPM2 generator, where high angular velocities are required to reach the voltage requirement, even in open circuit. For the RM1a generator, a minimum voltage requirement does not significantly affect the minimum wind required under 0.5V, as the voltage is not a constraint in this region of the design space.

Second, the effect of the minimum voltage and a maximum radius constraint on the minimum wind velocity is presented in Fig. 13 for the RPM2 and the Speed265 generators with a 20mW power requirement.

The minimum wind velocity is almost invariant with an increase in minimum voltage required for the Speed265 due to its highest k_v of all the generators considered in this study. Therefore, the minimum voltage is not a constraint within the current variable ranges. However, this configuration is strongly affected by a constraint on the maximum radius of the turbine. A large radius turbine allows capturing more energy, which reduces the minimum wind required, but also

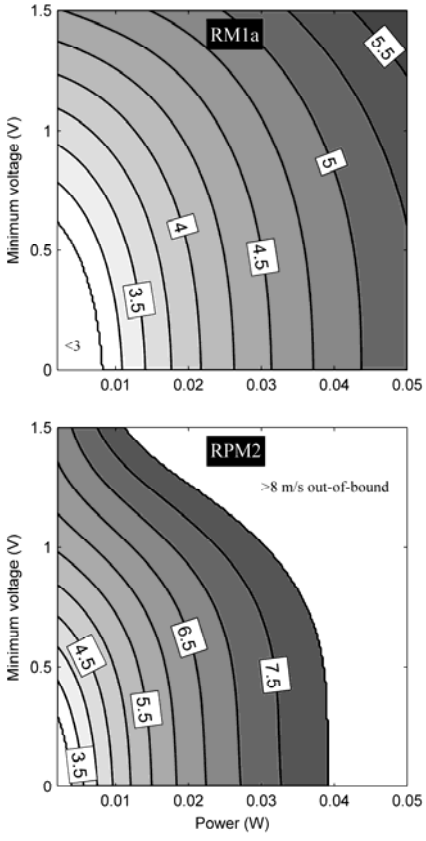


Fig. 12 Minimum wind required (m/s) as a function of power and minimum voltage for two generators

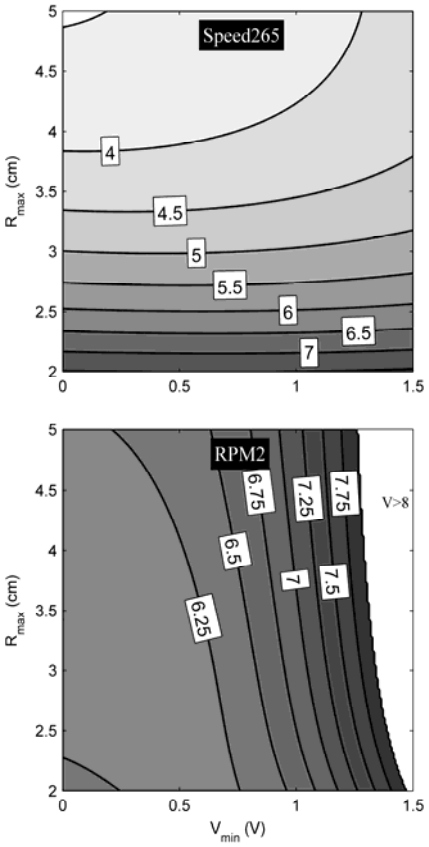


Fig. 13 Effect of the minimum voltage and maximum allowable radius on the required velocity (m/s) for 2 generators

https://doi.org/10.1017/jmech.2014.23 Published online by Cambridge University Press

reduces the angular velocity. For generators with a high electromagnetic constant, such as the Speed265, an increase in diameter leads to a reduction in the minimum wind required. For smaller generators such as the RPM2, the maximum radius is almost never a constraint; therefore the minimum wind velocity required is not affected. However, the minimum voltage requirement imposes a higher angular velocity which results in a smaller turbine and a significant increase in the minimum wind velocity.

Third, the effect of the minimum wind velocity as a function of the minimum voltage and the generator speed constant is presented in Fig. 14, for 20mW power requirement and using the regression on the generator friction presented in Fig. 5. The increase in the viscous drag friction coefficient K_F is assumed to be proportional to the change in T_0 with reference to the Speed265 generator.

High k_v generators can allow larger wind turbine at low angular velocity to reduce the wind required for a fixed power requirement, extending the design space. Smaller generators require higher wind velocities and are also affected by the minimum voltage required. Therefore, higher k_v generators are favorable even with the increase in friction for this specific case where 20mW is required.

Fourth, the optimal generators as a function of power required and minimum voltage required with a constrained radius is shown in Fig. 15 (R_{max} = 2cm), Fig. 16 (R_{max} = 2.5cm) and Fig. 17 (R_{max} = 3cm). The generator that leads to the lowest wind velocity required for each power-voltage combination is selected and presented in each figure (white font on black background). The dashed curves bound the regions of the design space where each generator is optimal. Sharp changes in the minimum velocity trends can be seen near the dashed curves due to the discrete change in the generator properties.

A constraint on the maximum radius significantly affects the optimal generator map. For a 2cm maximum radius constraint, the available torque for a fixed wind velocity is reduced. The optimal generators are small-size with low friction to extract power at high angular velocity and low torque, such as the RPM2 and the RPM1. However, it is impossible to produce over 45mW without exceeding the 8m/s upper limit on the wind velocity.

Relaxing the maximum radius constraint to 2.5cm extends the design space to turbines with higher torque, higher power, and lower angular velocity. This increase in available torque at lower angular velocity allows for high k_v generators to be more efficient even with the increase in friction. For high power levels, the wind velocity required drops under 8m/s.

The most favorable motor for a maximum radius constraint of 3 cm with voltage and power requirements of 1V and 20mW is the Speed265. However, for small power and low voltage requirements, small motors such as the RPM2 are still advantageous due to their low bearing friction. For unconstrained maximum radius, the Speed265 generator becomes the generator that allows the minimum wind velocity in the whole design space. Although counterintuitive, larger-size generators allows propeller designs to reduce the wind required, even for power generation of a few milliwatts.

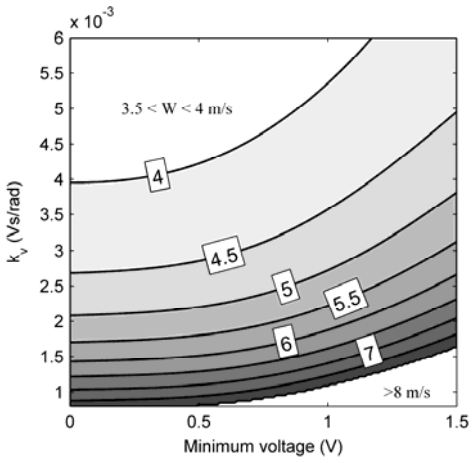


Fig 14 Minimum wind required (m/s) as a function of the minimum voltage requirement and k_v

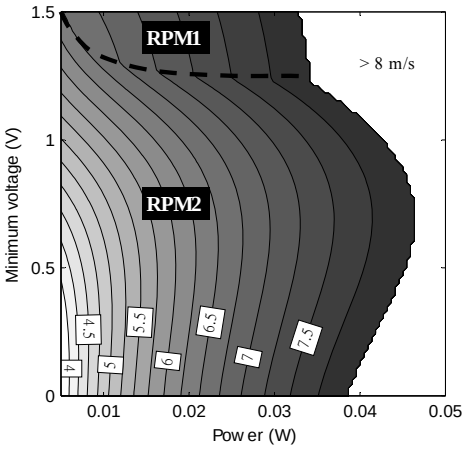


Fig. 15 Minimum wind required (m/s) and optimal generator as a function of power and minimum voltage with R_{max} = 2cm

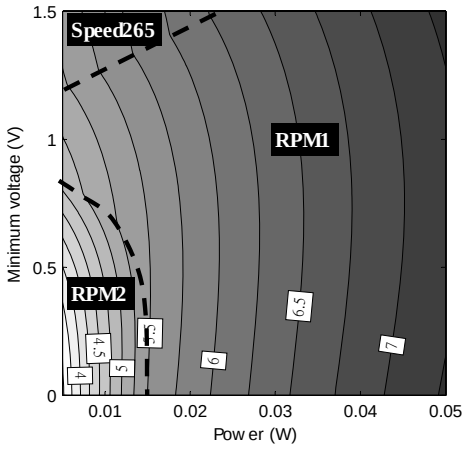


Fig. 16 Minimum wind required (m/s) and optimal generator as a function of power and minimum voltage with R_{max} = 2.5cm

https://doi.org/10.1017/jmech.2014.23 Published online by Cambridge University Press

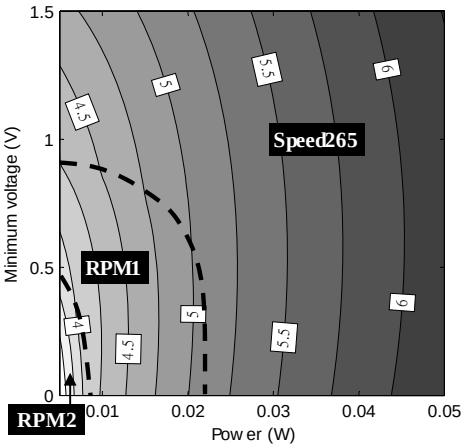


Fig. 17 Minimum wind required (m/s) and optimal generator as a function of power and minimum voltage with $R_{\max}$ = 3cm

7. CONCLUSIONS

This paper presented the design space exploration of a centimeter-scale wind turbine and DC generators to power sensors, using a calibrated physics-based model. On and off-design performances of the propeller alone showed the strong dependency of the available power to the airfoil zero-lift drag coefficient, design tip-speed ratio and operating condition. Several optimizations using a genetic algorithm are used to obtain a functional relationship between the minimum wind velocity and multiple constraints relevant to turbine designers, such as the maximum turbine radius, electrical power required, minimum voltage required and generator properties. The optimization formulation uses the results of previous optimizations to reduce the number of function calls based on the knowledge about the physics of the problem. It is shown that the favorable characteristics for micro DC generators are a high electromagnetic constant and low friction. However, as these parameters are positively correlated, large generators allow the lowest wind required only when large turbine can be used, even for low power generation. This approach to analyze micro wind turbines can also be extended to larger wind turbines, or even water turbines.

Future research should include the analysis of brushless AC motors for their high electromagnetic constant and absence of brushes as they could certainly increase the reliability and longevity of micro wind turbines. Also, an increase in the ranges of the design variables could allow a better understanding of the lower limit of the wind velocity for which power could be generated. However, a more detailed aerodynamic model should be implemented in the modeling and simulation environment to better represent the Reynolds numbers between 1,000 and 5,000 with variable thickness-to-chord ratio.

NOMENCLATURES

b	Number of blades
k_1	Penalty coefficient
k_t	Torque constant
k_v	Speed constant
Cd	Airfoil drag coefficient
Cd_0	Airfoil minimum drag
Cd_2	Airfoil lift-induced drag coefficient
Cl	Airfoil lift coefficient
Cl_α	Airfoil lift curve slope
Cl_0	Airfoil lift coefficient at zero angle of attack
Cl_{cd0}	Airfoil lift coefficient at minimum airfoil drag
Cl_{des}	Airfoil design lift coefficient
C_p	Power coefficient
i	Current
K_F	Viscous torque friction coefficient
P	Electrical power
P_{req}	Electrical power required
Re	Reynolds number
Re_{ref}	Reference Reynolds number
Re_{exp}	Correction factor for Reynolds number
R	Generator electrical resistance
r	Turbine radius
$r_{\max}$	Maximum turbine radius
T_0	Constant friction torque
T_f	Friction torque
T_m	Torque at the shaft
$U_{b,w}$	Lower bound on the wind velocity
V	Voltage
$V_{\min}$	Minimum voltage required
W	Wind velocity
W_d	Design wind velocity
	Tip-speed ratio (ωr / W)
λ_d	Design tip-speed ratio ($\omega_d r$ / W_d)
ω	Angular velocity
ω_d	Design angular velocity

APPENDIX A

Table 5 Generator properties

Motor	R (ohms)	k_v (Vs/rad)	T_0 (Nm)	K_f (Nms/rad)
Graupner — Speed265	8.11	0.00623	1.45E−4	9.64E−8
Solarbotics — TPM2	37.7	0.00052	4.37E−6	2.33E−9
Solarbotics — RPM2	10.8	0.00128	4.52E−6	8.41E−9
Solarbotics — RM1a	9.76	0.00440	1.03E−4	7.70E−8
Solarbotics — MK06-30	30.7	0.00124	6.30E−6	2.95E−9
Solarbotics — MK04s-10	12.0	0.000443	3.99E−6	2.57E−9
Solarbotics — MK04-40	37.2	0.000869	4.47E−6	2.23E−9

REFERENCES

1. Morais, R. S., Matos, G., Fernandes, M. A. A., Valente, L. G., Soares, S. F. S., Ferreira, P. P. J. S. G. and Reis, M. J. C. S., "Sun, Wind and Water Flow as Energy Supply for Small Stationary Data Acquisi-

https://doi.org/10.1017/jmech.2014.23 Published online by Cambridge University Press

tion Platforms," *Computers and Electronics in Agriculture*, **64**, pp. 120–132 (2008).
2. Nema, P., Nema, R. K. and Rangnekar, S., "A Current and Future State of Art Development of Hybrid Energy System Using Wind and PV-Solar: A Review," *Renewable and Sustainable Energy Reviews*, **13**, pp. 2096–2103 (2009).
3. Chen, H., Chou, P., Duri, S., Lei, H. and Reason, J., "The Design and Implementation of a Smart Building Control System," *2009 IEEE International Conference on E-Business Engineering*, Macau, pp. 255–262 (2009).
4. Sardini, E. and Serpelloni, M., "Passive and Self-Powered Autonomous Sensors for Remote Measurements," *Sensors*, **9**, pp. 943–960 (2009).
5. "ZL70250 Ultra-Low-Power Sub-GHz RF Transceiver," Microsemi Corporation (2012).
6. Vaussard, F., Bonani, M., Rétornaz, P., Martinoli, A. and Mondada, F., "Towards Autonomous Energy-Wise RObjects," *Proceedings of the 12th Conference Towards Autonomous Robotic Systems*, Sheffield, UK, pp. 311–322 (2011).
7. Widetronix, Available: http://www.widetronix.com/ [Accessed: 30-Oct-2012].
8. Sudevakatam, S. and Kulkarni, P., "Energy Harvest-Ing Sensor Nodes: Survez and Implications," *IEEE Communications Surveys and Tutorials*, **13**, pp. 443–461 (2011).
9. "Comparative Climate Data for the United States Through 2011," National Oceanic and Atmospheric Administration, Asheville, North Carolina, CCD-2011 (2011).
10. Judet de la Combe, A. and Sesolis, B., *Conception et calcul des installations de ventilation des bâtiments et des ouvrages*, Pyc éd, France (1992).
11. Gasch, R. and Twele, J. (Eds.), *Wind Power Plants: Fundamentals, Design, Construction and Operation*, 2nd Edition, 2012 Edition, Springer, Berlin Heidelberg (2011).
12. Hau, E. and Renouard, H., "Wind Turbines, Fundamentals, Technologies, Application, Economics," *Wind Turbines*, Springer, Berlin Heidelberg, pp. 91–160 (2006).
13. Federspiel, C. C. and Chen, J., "Air-Powered Sensor," *Proceedings of IEEE Sensors*, Toronto, Canada, pp. 22–25 (2003).
14. Rancourt, D., Tabesh, A. and Fréchette, L. G., "Evaluation of Centimeter-Scale Micro Wind Mills: Aerodynamics and Electromagnetic Power Generation," *Proceedings PowerMEMS*, Freiburg, Germany (2007).
15. Xu, F. J., Yuan, F. G., Hu, J. Z. and Qiu, Y. P., "Design of a Miniature Wind Turbine for Powering Wireless Sensors," *Proceedings of SPIE*, 7647, pp. 764741–764741–9 (2010).
16. Carli, D., Brunelli, D., Bertozzi, D. and Benini, L., "A High-Efficiency Wind-Flow Energy Harvester Using Micro Turbine," *Power Electronics Electrical Drives Automation and Motion (SPEEDAM), 2010 International Symposium*, pp. 778–783 (2010).
17. Vlad, C., Munteanu, I., Bratcu, A. I. and Ceangă, E., "Output Power Maximization of Low-Power Wind Energy Conversion Systems Revisited: Possible Control Solutions," *Energy Conversion and Management*, **51**, pp. 305–310 (2010).
18. Sardini, E. and Serpelloni, M., "Self-Powered Wireless Sensor for Air Temperature and Velocity Measurements with Energy Harvesting Capability," *Instrumentation and Measurement, IEEE Transactions*, **60**, pp. 1838–1844 (2011).
19. Flammini, A., Marioli, D., Sardini, E. and Serpelloni, M., "An Autonomous Sensor with Energy Harvesting Capability for Airflow Speed Measurements," *Instrumentation and Measurement Technology Conference (I2MTC), IEEE*, pp. 892–897 (2010).
20. Linear Technology, "LTC3108, Ultralow Voltage Step-Up Converter and Power Manager," 2012. [Online]. Available: http://cds.linear.com/docs/Datasheet/3108fb.pdf. [Accessed: 20-Nov-2012].
21. Holmes, A. S., Hong, Guodong. and Pullen, K. R., "Axial-Flux Permanent Magnet Machines for Micropower Generation," *Journal of Microelectromechanical Systems*, **14**, pp. 54–62 (2005).
22. Howey, D. A., Bansal, A. and Holmes, A. S., "Design and Performance of a Centimetre-Scale Shrouded Wind Turbine for Energy Harvesting," *Smart Materials and Structures*, **20**, p. 085021 (2011).
23. Myers, R. H., Montgomery, D. C. and Ander-son-Cook, C. M., *Response Surface Methodology: Process and Product Optimization Using Designed Experiments*, 3rd Edition, Wiley, New Jersey (2009).
24. Drela, M., "QPROP, Propeller/Windmill Analysis and Design," Dec-2007. [Online]. Available: http://web.mit.edu/drela/Public/web/qprop/. [Accessed: 01-Jul-2012].
25. Toliyat, H. A. and Kliman, G. B., *Handbook of Electric Motors*. CRC Press, Florida (2004).
26. Sunada, S., Sakaguchi, A. and Kawachi, K., "Airfoil Section Characteristics at a Low Reynolds Number," *Journal of Fluids Engineering*, **119**, p. 129 (1997).
27. Pelletier, A. and Mueller, T. J., "Low Reynolds Number Aerodynamics of Low-Aspect-Ratio, Thin/Flat/Cambered-Plate Wings," *Journal of Aircraft*, **37**, pp. 825–832 (2000).
28. Shyy, W., *Aerodynamics of Low Reynolds Number Flyers*, Cambridge University Press, Endland (2008).

(Manuscript received July 30, 2013,
accepted for publication December 19, 2013.)

https://doi.org/10.1017/jmech.2014.23 Published online by Cambridge University Press